Contribution from the Institut für Anorganische Chemie, Universität Bern, CH 3000 Bern 9, Switzerland, Laboratorium für Kristallographie, Universität Bern, CH 3012 Bern, Switzerland, and Institut de Chimie Minérale et Analytique, Université de Lausanne, CH 1005 Lausanne, Switzerland

Structure and Reactivity of Ruthenium Half-Sandwich Compounds: Crystal and Molecular Structure and Acetonitrile Exchange Kinetics and Mechanism of $Ru(\eta^6\text{-}C_6H_6)(CH_3CN)_3^{2+}$ and $Ru(\eta^5\text{-}C_5H_5)(CH_3CN)_3^{+}$

Werner Luginbühl,[1a] Pascal Zbinden,[1c] Pierre A. Pittet,[1c] Thomas Armbruster,[1b] Hans-Beat Bürgi,[1b] André E. Merbach,[1c] and Andreas Ludi*[,1a]

Received November 2, 1990

$[Ru(\eta^6\text{-}C_6H_6)(CH_3CN)_3](PF_6)_2$ crystallizes in the monoclinic space group $P2_1/c$ with a = 11.087 (3) Å, b = 12.779 (6) Å, c = 14.238 (10) Å, β = 100.44 (4)° (125 K), and Z = 4. The structure was refined to R = 0.022 for 3635 reflections with $I_o > 3\sigma(I_o)$. Average distances, corrected for thermal motion, are Ru–N = 2.059 (4) Å, Ru–C = 2.188 (2) Å, $(C\text{–}C)_{ring}$ = 1.408 (4) Å, N–C = 1.133 (3) Å, $(C\text{–}C)_{an}$ (an = acetonitrile) = 1.453 (1) Å, and Ru–center of ring = 1.675 Å. The torsional angle describing the relative arrangement of the benzene ring and the acetonitrile ligands is 12.2°. $[Ru(\eta^5\text{-}C_5H_5)(CH_3CN)_3]BF_4\cdot 0.5CH_3CN$ crystallizes in the monoclinic space group $I2/a$ with a = 23.684 (6) Å, b = 6.913 (2) Å, c = 21.550 (3) Å, β = 111.84 (1)° (296 K), and Z = 8. The structure was refined to R = 0.022 for 2226 reflections with $I_o > 3\sigma(I_o)$. After correction for thermal motion average distances are Ru–N = 2.090 (1) Å, Ru–C = 2.141 (2) Å, $(C\text{–}C)_{ring}$ = 1.396 (7) Å, N–C = 1.135 (3) Å, $(C\text{–}C)_{an}$ = 1.450 (4) Å, and Ru–center of ring = 1.781 Å. Acetonitrile exchange rates at variable temperature and pressure were determined by ^1H NMR spectroscopy. For $Ru(\eta^6\text{-}C_6H_6)(CH_3CN)_3^{2+}$ the results are $k(298\ K) = 4.07 \times 10^{-5}\ s^{-1}$, $\Delta H^{\ddagger}$ = 102.5 kJ mol^{-1}, $\Delta S^{\ddagger}$ = 15.0 J K^{-1} mol^{-1}, and $\Delta V^{\ddagger}$ = 2.4 cm^3 mol^{-1}; for $Ru(\eta^5\text{-}C_5H_5)(CH_3CN)_3^{+}$ $k(298\ K) = 5.6\ s^{-1}$, $\Delta H^{\ddagger}$ = 86.5 kJ mol^{-1}, $\Delta S^{\ddagger}$ = 59.6 J K^{-1} mol^{-1}, and $\Delta V^{\ddagger}$ = 11.1 cm^3 mol^{-1}. For the benzene compound an interchange mechanism (I) applies whereas for the $C_5H_5^-$ species a dissociative pathway (D) is followed. The correlation between structural properties and kinetic behavior is discussed in terms of a simple bonding model.

Introduction

Arene and cyclopentadienyl compounds of ruthenium are a well-established family of robust metal–organic molecules that played an important role in the development of organometallic chemistry.[2] For the two parent compounds $Ru(\eta^6\text{-}C_6H_6)_2^{2+}$ and $Ru(\eta^5\text{-}C_5H_5)_2$ and their numerous derivatives a wealth of information on synthesis and general properties is available.[2] The corresponding half-sandwich or piano-stool complexes $Ru(\eta^6\text{-}C_6H_6)L_3^{2+}$ and $Ru(\eta^5\text{-}C_5H_5)L_3^{+}$ have been studied only occasionally.[3] These species represent interesting conceptual links between classical Werner complexes and organometallic molecules, since they combine the two prototypical coordinative environments within one single mononuclear unit. This combination of the two generally incompatible moieties is most conspicuously illustrated by the ion $Ru(\eta^6\text{-}C_6H_6)(H_2O)_3^{2+}$.[4]

In addition to the rich structural chemistry of ruthenium compounds, particularly with π-acids, substitution rates and mechanisms have been investigated for quite a number of ruthenium complexes, the $Ru(NH_3)_5L^{2+}$ ion being a particularly well-studied example.[5] According to the general pattern, substitution on Ru(II) proceeds by an interchange pathway, whereas an associative mechanism applies for Ru(III) complexes. Hexacoordinated Ru(II) compounds span about 10 orders of magnitude in their substitution labilities. For these systems the trend in substitution rates correlates with the extent of back-bonding, e.g. moderately fast ligand exchange for H_2O and very inert behavior for CH_3CN.[6] While some of the half-sandwich compounds have been shown to be efficient starting reagents for synthetic work,[3,7] very few kinetic data exist for these systems. Their borderline position between coordination and organometallic chemistry led us to include them in our studies on structure and reactivity of ruthenium compounds. This paper reports the molecular structures, ligand-exchange kinetics, and the discussion of the substitution pathway for $Ru(\eta^6\text{-}C_6H_6)(CH_3CN)_3^{2+}$ and $Ru(\eta^5\text{-}C_5H_5)(CH_3CN)_3^{+}$.

Experimental Section

A. Preparation and Crystal Growth. Published procedures were used to prepare $[Ru(\eta^6\text{-}C_6H_6)(CH_3CN)_3](PF_6)_2$ (I)[3] and $[Ru(\eta^5\text{-}C_5H_5)(CH_3CN)_3]BF_4\cdot 0.5CH_3CN$ (II).[7]

A 100-mg sample of I was dissolved in 8 mL of acetone, and the solution was placed in a desiccator over ether. Isothermal distillation of ether into the acetone solution produced pseudohexagonal platelike crystals within 3–5 days. The yellow crystals are air stable and can be dissolved in a variety of solvents such as acetonitrile, acetone, and ethanol without decomposition.

A saturated solution of II at 30 °C was prepared by adding 6 mL of acetonitrile–1,2-dichloroethane (1:4, v/v) to a slurry of 30 mg of II in 15 mL of cyclohexane. This solution was transferred by syringe into a Schlenk vessel. Slow cooling to 4 °C produced yellow prismatic crystals within 2–3 days. Because II is very air sensitive, all the operations were carried out under Ar. The isolated crystals turn black also under Ar or N_2 and can be stored without decomposition only in contact with the solvent mixture. For this reason crystals for the X-ray study were sealed in Lindemann capillaries together with a small amount of solvent. The PF_6 salt can also be obtained as yellow crystals, which are considerably more stable. However, their precession and Weissenberg photographs show diffraction lines in between layers of the reciprocal lattice, indicative of a highly disordered structure.

B. Crystal Structure Analysis of $[Ru(\eta^6\text{-}C_6H_6)(CH_3CN)_3](PF_6)_2$ (I) and $[Ru(\eta^5\text{-}C_5H_5)(CH_3CN)_3]BF_4\cdot 0.5CH_3CN$ (II). Lattice parameters (Table I) were determined by least-squares optimization of 14 accurately centered reflections in the θ range 11.7–15° (I) and 20.8–21.6° (II). The space group $I2/a$ (II) was preferred over the conventional $C2/c$ to avoid an unnecessary small monoclinic angle and ensuing intrinsic correlation between the atomic x and z coordinates. Intensities were measured with

(1) (a) Institut für Anorganische Chemie, Universität Bern. (b) Laboratorium für Kristallographie, Universität Bern. (c) Institut de Chimie Minérale et Analytique, Université de Lausanne.
(2) Bennett, M. A.; Bruce, M. I.; Matheson, T. W. In *Comprehensive Organometallic Chemistry*; Wilkinson, G., Ed.; Pergamon: Oxford, England, 1982; Vol. 4.
(3) (a) Bennett, M. A.; Smith, A. K. *J. Chem. Soc., Dalton Trans.* **1974**, 233. (b) Stebler-Röthlisberger, M.; Ludi, A. *Polyhedron* **1986**, *5*, 1217.
(4) (a) Hung, Y.; Kung, W.; Taube, H. *Inorg. Chem.* **1981**, *20*, 457. (b) Stebler-Röthlisberger, M.; Hummel, W.; Pittet, P. A.; Bürgi, H. B.; Ludi, A.; Merbach, A. E. *Inorg. Chem.* **1988**, *27*, 1358.
(5) Taube, H. *Comments Inorg. Chem.* **1981**, *1*, 17.
(6) Rapaport, I.; Helm, L.; Merbach, A. E.; Bernhard, P.; Ludi, A. *Inorg. Chem.* **1988**, *27*, 873.
(7) (a) Gill, T. P.; Mann, K. R. *Organometallics* **1982**, *1*, 485. (b) Werner, H.; Werner, R. *Chem. Ber.* **1984**, *117*, 142. (c) McNair, A. M.; Mann, K. R. *Inorg. Chem.* **1986**, *25*, 2519. (d) Schrenk, J. L.; McNair, A. M.; McCormick, F. B.; Mann, K. R. *Inorg. Chem.* **1986**, *25*, 3501. (e) McNair, A. M.; Boyd, D. C.; Mann, K. R. *Organometallics* **1986**, *5*, 303. (f) Sauer, N. N.; Angelici, R. J. *Organometallics* **1987**, *6*, 1146. (g) Moriarty, R. M.; Ku, Y.-Y.; Gill, U. S. *J. Chem. Soc., Chem. Commun.* **1987**, 1837. (h) Fish, R. H.; Kim, H.-S.; Fong, R. H. *Organometallics* **1989**, *8*, 1375.

0020-1669/91/1330-2350$02.50/0

Table I. Crystallographic Data for $[Ru(\eta^6\text{-}C_6H_6)(CH_3CN)_3](PF_6)_2$ (I) and $[Ru(\eta^5\text{-}C_5H_5)(CH_3CN)_3]BF_4\cdot 0.5CH_3CN$ (II)

	I	II
formula	$C_{12}H_{15}N_3P_2F_{12}Ru$	$C_{12}H_{15.5}N_{3.5}BF_4Ru$
fw	592.27	396.65
a, Å	11.087 (3)	23.684 (6)
b, Å	12.779 (6)	6.913 (2)
c, Å	14.238 (10)	21.550 (3)
β, deg	100.44 (4)	111.84 (1)
V, Å^3	1983.8	3275.2
space group	$P2_1/c$ (No. 14)	$I2/a$ (No. 15)
Z	4	8
D_{obs} (flotation), g cm^{-3}	1.882 (1)	1.604 (1)
D_{calc}, g cm^{-3}	1.892	1.609
cryst dimens, mm	0.23 × 0.16 × 0.14[a] 0.20 × 0.15 × 0.12	0.44 × 0.22 × 0.11
μ, cm^{-1}	10.45	8.87
transm coeff	0.75–0.88	0.94–1
h,k,l	0–14,0–16,$\overline{18}$–18	$\overline{29}$–29,0–8,0–26
T, K	125	296
scan width, deg	1 + 0.3 tan θ	0.8 + 0.35 tan θ
scan mode	ω	ω–2θ
no. of unique reflcns measd	4284	2904
no. of unique reflcns measd with $I_o > 3\sigma(I_o)$	3635	2226
R	0.022	0.022
R_w	0.023	0.032
goodness of fit	1.22	1.27
final shift/error	0.05	0.06[b]

[a] This crystal cracked after collection of the first 1713 reflections. Further data collection was done with a second crystal. The two data sets were combined and appropriately scaled for further processing. [b] 0.59 for the disordered F atoms, 0.14 for H atoms.

a CAD-4 diffractometer using graphite-monochromatized Mo Kα radiation (λ = 0.71069 Å). The standard liquid-nitrogen attachment was used for data collection of I at 125 K. Compound II was studied at room temperature, since at low temperature the unavoidable solvent around the crystal solidifies and leads to unmanageable high background and to additional reflections. No systematic intensity fluctuations were observed for the three check reflections recorded every 60 min for I and II. The orientation of II was controlled and, if necessary, corrected after at most every 100 reflections to account for slight crystal movements within the liquid. Intensities were corrected for Lorentz–polarization effects. An empirical absorption correction[8] was applied for II but none for I. Neutral-atom scattering factors were employed, including anomalous dispersion for all non-hydrogen atoms.[9] Further information concerning crystal data, intensity collection, and refinement is given in Table I.

The SDP program system[8] was used on a PDP 11/34 computer for data reduction and for solving and refining the structure of I. The structure of II was solved and refined by using the SHELX76 package[10] on a IBM 3080/180 computer. ORTEP drawings were generated with XTAL2.4[11] program, and thermal motion analysis was performed with the programs THMV and THMA11.[12]

Both crystal structures were solved by Patterson and Fourier methods. Hydrogen positions were either generated or located in ΔF maps. The non-hydrogen atoms were refined anisotropically; the hydrogen atoms, isotropically. Two different isotropic thermal parameters were assigned to the hydrogens of I, the ring and methyl H's being treated as two separate groups. Hydrogens were given individual B's for II. The function $\sum w(|F_o| - |F_c|)^2$ was minimized with w = 1 for I (other weighting schemes produced poorer agreement) and $w = 1/(\sigma^2(F_o) + 0.000533F_o^2)$ for II. Intermediate ΔF maps for II revealed significant peaks in the coordination shell of the BF_4^- anion. The apparent disorder could be partly resolved by introducing two positions for the F atoms (F1–F4 and FA–FD; see Table III) with variable population parameters. Their sum was constrained to unity. No improvement could be obtained with a third orientation of the BF_4^- unit although final ΔF maps showed corresponding residual peaks of ≤0.3 e Å^{-3}. Final ΔF maps showed residual peaks of +0.48 and −0.59 e Å^{-3} close to the N3 position for I and +0.31 and −0.25 e Å^{-3} close to the Ru position for II.

Table II. Final Atomic Positional Parameters and B_{eq} Values, with Standard Deviations in Parentheses, for $[Ru(\eta^6\text{-}C_6H_6)(CH_3CN)_3](PF_6)_2$ (I)

atom	x/a	y/b	z/c	B_{eq},[a] Å^2
Ru	0.19672 (2)	0.46629 (1)	0.80962 (1)	1.154 (2)
N1	0.3707 (2)	0.4237 (2)	0.8754 (1)	1.58 (3)
N2	0.2543 (2)	0.4371 (2)	0.6834 (1)	1.76 (3)
N3	0.2661 (2)	0.6140 (2)	0.7966 (1)	1.46 (3)
C1	−0.0005 (2)	0.4689 (2)	0.7525 (2)	2.33 (4)
C2	0.0240 (2)	0.5351 (2)	0.8317 (2)	2.60 (5)
C3	0.0888 (2)	0.4988 (2)	0.9205 (2)	2.41 (4)
C4	0.1278 (2)	0.3950 (2)	0.9285 (2)	2.12 (4)
C5	0.1040 (2)	0.3262 (2)	0.8492 (2)	1.92 (4)
C6	0.0405 (2)	0.3639 (2)	0.7619 (2)	1.99 (4)
C7	0.4624 (2)	0.3931 (2)	0.9133 (2)	1.62 (3)
C8	0.5794 (2)	0.3532 (2)	0.9629 (2)	2.30 (4)
C9	0.2789 (3)	0.4195 (2)	0.6117 (2)	2.28 (4)
C10	0.3069 (4)	0.3957 (3)	0.5184 (2)	4.30 (7)
C11	0.2984 (2)	0.6970 (2)	0.7866 (2)	1.53 (3)
C12	0.3378 (3)	0.8038 (2)	0.7762 (2)	2.15 (4)
P1	0.11572 (6)	0.68577 (5)	0.51842 (4)	1.532 (8)
P2	0.33475 (6)	0.38777 (5)	0.21451 (4)	1.630 (9)
F1	0.2531 (1)	0.6540 (1)	0.5663 (1)	2.41 (2)
F2	0.1655 (2)	0.7313 (2)	0.4277 (1)	3.18 (3)
F3	0.1360 (1)	0.7988 (1)	0.5680 (1)	2.37 (3)
F4	−0.0206 (1)	0.7191 (1)	0.4699 (1)	2.72 (3)
F5	0.0658 (1)	0.6426 (1)	0.6087 (1)	2.61 (2)
F6	0.0969 (2)	0.5743 (1)	0.4682 (1)	3.13 (3)
F7	0.4432 (2)	0.4680 (2)	0.2485 (2)	4.11 (4)
F8	0.4047 (2)	0.3012 (1)	0.2837 (1)	3.88 (3)
F9	0.2675 (2)	0.4286 (2)	0.2967 (1)	4.29 (4)
F10	0.2253 (2)	0.3094 (1)	0.1793 (2)	4.29 (4)
F11	0.2633 (2)	0.4747 (1)	0.1446 (1)	3.00 (3)
F12	0.4020 (2)	0.3480 (2)	0.1314 (1)	4.88 (4)

[a] The isotropic equivalent thermal parameter B_{eq} is defined as $B_{eq} = {}^8/_3\pi^2\sum_i(\sum_j(U_{ij}a_i^*a_j^*a_ia_j))$.

Table III. Final Atomic Positional Parameters and B_{eq} Values, with Standard Deviations in Parentheses, for $[Ru(\eta^5\text{-}C_5H_5)(CH_3CN)_3]BF_4\cdot 0.5CH_3CN$ (II)

atom	x/a	y/b	z/c	B_{eq},[a] Å^2
Ru	0.37010 (1)	−0.11990 (3)	0.20780 (1)	3.560 (3)
N1	0.2968 (1)	0.0707 (4)	0.1833 (1)	4.06 (4)
N2	0.4006 (1)	0.0529 (4)	0.1475 (1)	4.13 (4)
N3	0.4173 (1)	0.0622 (4)	0.2872 (1)	4.09 (4)
C1	0.3922 (3)	−0.3742 (6)	0.2683 (2)	6.5 (1)
C2	0.4187 (3)	−0.3870 (6)	0.2202 (3)	7.1 (1)
C3	0.4711 (3)	−0.3857 (6)	0.1572 (3)	7.5 (1)
C4	0.3172 (3)	−0.3712 (6)	0.1668 (3)	7.8 (1)
C5	0.3300 (3)	−0.3634 (6)	0.2358 (3)	7.3 (1)
C6	0.2535 (1)	0.1603 (5)	0.1661 (2)	4.25 (5)
C7	0.1979 (2)	0.2700 (9)	0.1438 (3)	6.2 (1)
C8	0.4136 (2)	0.1404 (4)	0.1108 (2)	4.29 (5)
C9	0.4309 (3)	0.2508 (8)	0.0632 (3)	6.7 (1)
C10	0.4432 (1)	0.1457 (5)	0.3344 (2)	4.17 (5)
C11	0.4774 (2)	0.2483 (7)	0.3952 (2)	5.78 (8)
B	0.8861 (1)	0.2494 (5)	0.4464 (2)	4.38 (6)
F1	0.8833 (4)	0.272 (2)	0.5070 (3)	8.3 (2)
F2	0.8336 (3)	0.283 (2)	0.3979 (4)	9.9 (2)
F3	0.9275 (3)	0.374 (1)	0.4423 (4)	9.1 (2)
F4	0.9074 (4)	0.0727 (8)	0.4438 (5)	9.7 (2)
FA	0.9298 (6)	0.155 (3)	0.4358 (6)	17.9 (6)
FB	0.8788 (6)	0.178 (3)	0.4999 (5)	12.6 (4)
FC	0.9001 (9)	0.432 (1)	0.4570 (8)	17.7 (6)
FD	0.8342 (4)	0.234 (2)	0.3931 (5)	9.9 (3)
C12	0.25	0.158 (2)	0.0	7.9 (2)
C13	0.25	−0.045 (3)	0.0	9.4 (4)
N4	0.25	0.317 (2)	0.0	13.2 (3)

[a] The isotropic equivalent thermal parameter B_{eq} is defined as $B_{eq} = {}^8/_3\pi^2\sum_i(\sum_j(U_{ij}a_i^*a_j^*a_ia_j))$.

(8) Frenz, B. A. *Structure Determination Package*; Enraf-Nonius: Delft, The Netherlands, 1983.
(9) Cromer, D. T.; Waber, J. T. *International Tables for X-Ray Crystallography*; Kynoch: Birmingham, England, 1974; Vol. IV, Table 2.2.B.
(10) Sheldrick, G. SHELX76. Program for Crystal Structure Determination. University of Cambridge, England, 1976.
(11) ORTEP. Version of G. Davenport and S. R. Hall in XTAL2.4. Hall, S. R., Stewart, J. M., Eds.; Universities of Western Australia and Maryland, 1988.
(12) Trueblood, K. N. THMV9 and THMA11. Thermal Motion Analysis. University of California, Los Angeles, CA, 1985, 1987.

Table IV. Temperature and Pressure Dependence of the CH_3CN Exchange Rate Constant, k, on $Ru(\eta^6\text{-}C_6H_6)(CH_3CN)_3^{2+}$ and $Ru(\eta^5\text{-}C_5H_5)(CH_3CN)_3^{+}$ [a]

$Ru(\eta^6\text{-}C_6H_6)(CH_3CN)_3^{2+}$ [b]				$Ru(\eta^5\text{-}C_5H_5)(CH_3CN)_3^{+}$ [c]			
T, K	10^5k, s^{-1}	P, MPa	10^5k, s^{-1}	T, K [d]	k, s^{-1}	P, MPa [e]	k, s^{-1}
295.2	3.0	0.1	12.2	287.6	1.5	0.1	38.5
298.2	3.9	40.0	12.2	295.1	4.1	0.1	40.4
303.2	7.7	120.0	10.5	304.6	10.8	35.0	34.1
308.2	14.8	158.0	9.8	309.6	22.8	50.0	32.9
313.2	32.5	200.0	10.3	313.7	33.2	50.0	34.7
318.2	62.2			321.0	73.3	77.0	29.1
						100.0	27.4
						102.0	27.1
						126.0	23.8
						150.0	21.2
						170.0	18.8
						181.0	19.0

[a] Concentration of complex: 0.1 m. [b] Variable-temperature study at 400 MHz, variable-pressure study at 304.6 K and 200 MHz; neat solvent. [c] At 400 MHz. Variable-pressure study at 314.7 K. [d] CH_3CN–CD_3CN, 1:1. [e] CH_3CN–CD_3CN, 1:4.

The refined atomic coordinates for the two structures are listed in Tables II and III.

C. Acetonitrile Exchange Kinetics on $Ru(\eta^6\text{-}C_6H_6)(CH_3CN)_3^{2+}$ and $Ru(\eta^5\text{-}C_5H_5)(CH_3CN)_3^{+}$. CD_3NO_2 and CD_3CN (Ciba-Geigy, 99.0 atom % D) were dried over 3-Å molecular sieves. CH_3CN was distilled 3 times over P_2O_5. The solutions used for the NMR kinetic experiments were prepared by weighing, and all chemical shifts were referred to TMS. For all the kinetic experiments PF_6^- salts of both complex ions were used.

The ^1H NMR spectra were recorded with wide-bore Bruker CXP-200 (4.7 T) and Bruker AM-400 (9.4 T) spectrometers. Ordinary 5-mm o.d. tubes were employed for the ambient pressure measurements, and the deuterium signal of the solvent was used as a lock. For the variable-pressure measurements up to 200 MPa, two high-pressure probes were used, either with the CXP-200[13] (without lock) or with the AM-400[14] (with lock) spectrometer. The temperature was held constant by using a Bruker B-VT 1000 instrument within ±0.4 K (variable temperature) or by pumping a thermostated liquid (±0.2 K, variable pressure). The temperature was measured by using MeOH as a calibrant or by using a substitution technique[15] and a built-in Pt resistor,[16] respectively.

The very slow exchange of CH_3CN on $Ru(\eta^6\text{-}C_6H_6)(CH_3CN)_3^{2+}$

$$Ru(\eta^6\text{-}C_6H_6)(CH_3CN)_3^{2+} + 3CD_3CN \rightarrow Ru(\eta^6\text{-}C_6H_6)(CD_3CN)_3^{2+} + 3CH_3CN \quad (1)$$

was followed by monitoring the increase in intensity of the proton NMR signal of the free CH_3CN (at +1.97 ppm) and the decrease of the bound CH_3CN (at +2.50 ppm). The spectra were taken after mixing the complex and deuterated acetonitrile, as soon as the temperature and the pressure were stable, at regular intervals of time on a spectral width of 2600 Hz, with 30–50 scans recorded on 4K data points with a 10-s repetition rate. The time dependence of the mole fraction x of bound CH_3CN, obtained by integration of the signals, was fitted to eq 2,[17] where

$$x = x_{inf} + (x_0 - x_{inf}) \exp[-kt/(1 - x_{inf})] \quad (2)$$

x_0 (x at $t = 0$) and k (the rate constant for the exchange of a particular solvent molecule[18]) were the adjustable parameters and $x_{inf} \approx 3 \times 0.1 \times M(CD_3CN)/1000 \approx 0.013$ is obtained from the molality of the complex. The variable-temperature and variable-pressure k data (Table IV) were then analyzed according to eqs 3 and 4, respectively. The aceto-

$$k = (k_B T/h) \exp(\Delta S^*/R - \Delta H^*/RT) \quad (3)$$

$$\ln k_p = \ln k_0 - P\Delta V^*/RT \quad (4)$$

nitrile exchange on $Ru(\eta^5\text{-}C_5H_5)(CH_3CN)_3^{+}$ is faster and can be followed by the line-broadening method. At low temperature the signal of bound acetonitrile (at +2.35 ppm) is narrow and well separated from that of free acetonitrile. In a CH_3CN–CD_3CN mixture line broadening of the

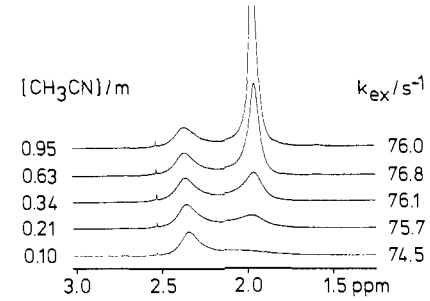

Figure 1. Experimental ^1H NMR (200 MHz) spectra of $Ru(\eta^5\text{-}C_5H_5)(CH_3CN)_3^{+}$, 0.1 m in the diluent CD_3NO_2, with various concentrations of CH_3CN at 323.0 K. On the left side is the signal of bound CH_3CN (+2.35 ppm), and on the right side is the signal of free CH_3CN (+1.97 ppm). Spectra were taken on a spectral width of 2000 Hz, with 30 scans recorded on 8K data points with a 10-s repetition rate.

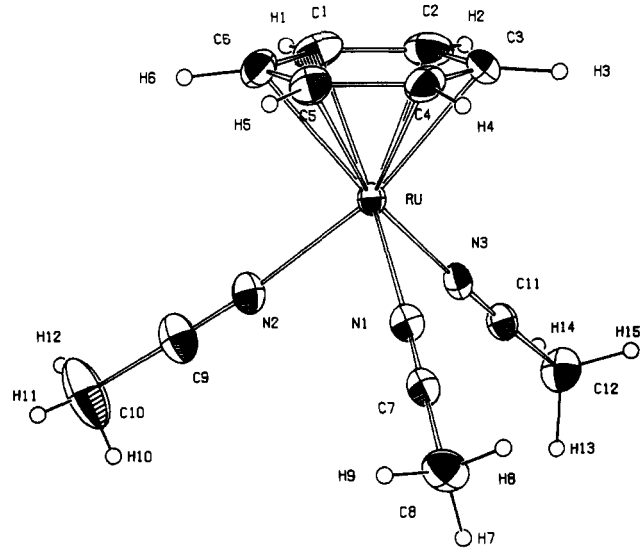

Figure 2. Molecular structure of $Ru(\eta^6\text{-}C_6H_6)(CH_3CN)_3^{2+}$.

bound signal starts at about 280 K (Table IV). The line width at half-height, $\Delta\nu_{1/2}$ (Hz), of the signal obtained by a least-squares fitting to a Lorentzian curve is related to the transverse relaxation rate of the bound acetonitrile proton, $1/T_2^b$ (s^{-1}), and in the limit of slow exchange[19] to k the exchange rate constant by eq 5. The variable-temperature (varia-

$$1/T_2^b = \pi(\Delta\nu_{1/2}) = k \quad (5)$$

ble-pressure) spectra of 1300–2000 Hz (1500 Hz) total width were obtained by Fourier transformation of the free induction decay (FID) accumulated with 30–2000 (40–200) scans on 8–16 K (16K) data points with a 10-s repetition rate. Data analysis (Table IV) again followed eqs 3 and 4.

For $Ru(\eta^5\text{-}C_5H_5)(CH_3CN)_3^{+}$, the free acetonitrile concentration dependence of the exchange rate constant k was studied in the inert diluent CD_3NO_2. The experimental spectra and rate constants obtained from least-squares fitting of the spectra by using the Kubo–Sack method[20] are reported in Figure 1. It is clear that k is independent on the concentration of free acetonitrile ($k = 75.2 \pm 0.7$ s^{-1} at 323.0 K).

Results and Discussion

A. Molecular Structures of $Ru(\eta^6\text{-}C_6H_6)(CH_3CN)_3^{2+}$ and $Ru(\eta^5\text{-}C_5H_5)(CH_3CN)_3^{+}$. The overall geometry for both complex ions corresponds to the characteristic piano-stool configuration, molecule I showing the expected approximate C_3 symmetry (Figures 2 and 3). For both compounds the aromatic ring is planar and the largest deviations from the carbon atom least-squares plane are 0.004 (3) Å (I) and 0.003 (4) Å (II). As observed in related structures,[4b,21] the aromatic C–H bonds are bent umbrella-like toward the metal center. Spacings between

(13) Pisaniello, D. L.; Helm, L.; Meier, P.; Merbach, A. E. *J. Am. Chem. Soc.* **1983**, *105*, 4258.
(14) Frey, U.; Helm, L.; Merbach, A. E. *High-Pressure Res.* **1990**, *2*, 237.
(15) Ammann, C.; Meier, P.; Merbach, A. E. *J. Magn. Reson.* **1982**, *46*, 319.
(16) Meyer, F. K.; Merbach, A. E. *J. Phys. E* **1979**, *12*, 185.
(17) Helm, L.; Elding, L. I.; Merbach, A. E. *Inorg. Chem.* **1985**, *24*, 1719.
(18) Swaddle, T. W. *Adv. Inorg. Bioinorg. Mech.* **1983**, *2*, 95.
(19) McLaughlin, A. C.; Leigh, J. S. *J. Magn. Reson.* **1973**, *9*, 296.
(20) Delpuech, J.-J.; Ducom, J.; Michon, V. *Bull. Chem. Soc. Fr.* **1971**, 1848.
(21) Beck, U.; Hummel, W.; Bürgi, H. B.; Ludi, A. *Organometallics* **1987**, *6*, 20.

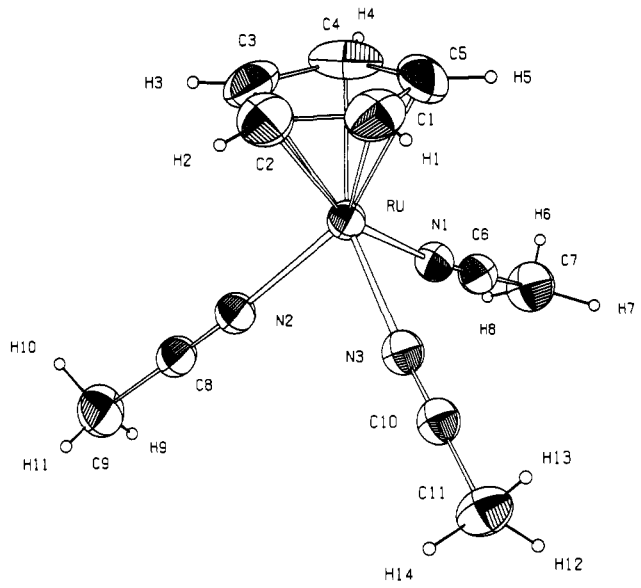

Figure 3. Molecular structure of $Ru(\eta^5\text{-}C_5H_5)(CH_3CN)_3^+$.

the C and H plane are 0.09 and 0.04 Å, respectively.

The planes defined by the aromatic carbon rings, the attached hydrogens, the nitrogens, and the two different carbon atoms of the three acetonitrile ligands form an almost perfect parallel stack. The largest deviation from parallel arrangement is 1.6° (I) and 3.3° (II).

Important interatomic distances and angles are listed in Table V. Average distances and angles are displayed in Figure 4. For I we observe a significant alternation in the benzene C–C distances. Thermal motion correction[12] was done on the basis of a nonrigid body model including internal rotation of C_6H_6 about an axis defined by Ru and the center of C_6H_6. Inclusion of benzene rotation improved the rigid body R factor from 10.2 to 6.9% and gave a mean square rotation amplitude for C_6H_6 of 33.2 (2.4) deg^2. Corrected C–C distances are 1.425 (1) and 1.405 (2) Å for the long and short bond lengths, respectively. In the projection along the pseudo C_3 axis the Ru–N bonds intersect the long C–C distances. A similar but smaller fluctuation is shown by the Ru–C distances. Analogous bond length variations are found for the $C_5H_5^-$ fragment in II (Table V). The average of the two short C–C bond lengths is 1.421 (1) Å, and that of the three long ones, 1.450 (1) Å; both values are corrected for thermal motion by using an analogous model of motion (amplitude of $C_5H_5^-$ is 199 deg^2). In the projection perpendicular to C_5H_5 the Ru–N bonds intersect the long C–C bonds (Figure 4).

Comparison of I and II with the parent molecules $Ru(C_6H_6)_2^{2+}$ [21] and $Ru(C_5H_5)_2$ [22] and with $Ru(CH_3CN)_6^{2+}$ [23] shows evidence for mutual (trans) influence of ligands. The corrected Ru–C distances in I and II are shorter by 0.037 and 0.048 Å and the corrected Ru–N distances longer by 0.030 and 0.061 Å than the corrected distances in the reference compounds. The corrected average C–C distances in I and II contract by 0.010 and 0.037 Å relative to the parent sandwich compounds.[21,22]

The $Ru(CH_3CN)_3$ moieties in I and II are very similar; the acetonitrile ligands, i.e. the legs of the piano stool, are slightly curved away from the central axis of the molecule (torsion angles N–C–Ru–ring center vary between −48 and 32° for I and between −29 and 61° for II). In the projection along this axis the N–Ru–N angles are close to the ideal value of 120°; the largest deviation is 2.2° for I and 2.5° for II.

Within the crystal the $Ru(\eta^6\text{-}C_6H_6)(CH_3CN)_3^{2+}$ ions are arranged approximately as sheets along the bc plane with all the acetonitrile ligands sticking out on both sides of this pseudoplane containing the benzene molecules (Figure 5). The PF_6^- counterions are filling the cavities between acetonitrile molecules of this double layer. They show virtually octahedral symmetry with an average P–F distance of 1.594 (2) Å.

The $Ru(\eta^5\text{-}C_5H_5)(CH_3CN)_3^+$ complex ions in the crystal of II are oriented with their molecular axis parallel to the b axis, pairwise connected by a center of symmetry between two molecules (Figure 6). The two disordered tetrahedral BF_4^- units in this rather open lattice are related by an approximate local mirror plane at $y \sim 0.25$. The average B–F distance is 1.325 (5) Å.

B. Kinetic Results and Mechanisms. The results of the kinetic measurements at variable temperature and pressure (Figure 7) evaluated by using eqs 3 and 4 are summarized in Table VI. We notice a dramatic rate enhancement by 5 orders of magnitude from $Ru(\eta^6\text{-}C_6H_6)(CH_3CN)_3^{2+}$ to $Ru(\eta^5\text{-}C_5H_5)(CH_3CN)_3^+$ and, more importantly, an increase in ΔS^* and ΔV^*. An enthalpy term ($\Delta\Delta H^* = 16.0$ kJ mol^{-1}) as well as an entropy term ($T\Delta\Delta S^* = 13.3$ kJ mol^{-1}) contributes to this rate enhancement. The values obtained for ΔV^* in particular present clear evidence for the nature of the exchange pathway for the two complex ions. Whereas an interchange mechanism applies for the benzene complex, replacement of the $\eta^6\text{-}C_6H_6$ fragment by $\eta^5\text{-}C_5H_5^-$ turns the acetonitrile exchange into a dissociative pathway (large positive ΔV^* and first-order rate law). The difficulties encompassed in the crystal growing experiments find a simple explanation in the high substitution lability of acetonitrile in $Ru(\eta^5C_5H_5)(CH_3CN)_3^+$.

The substitution lability for acetonitrile increases along the series $Ru(CH_3CN)_6^{2+}$, $Ru(\eta^6\text{-}C_6H_6)(CH_3CN)_3^{2+}$, $Ru(\eta^5\text{-}C_5H_5)$-

Table V. Important Interatomic Distances (Å) and Angles (deg) for the Complex Ions $Ru(\eta^6\text{-}C_6H_6)(CH_3CN)_3^{2+}$ and $Ru(\eta^5\text{-}C_5H_5)(CH_3CN)_3^+$ [a]

$Ru(\eta^6\text{-}C_6H_6)(CH_3CN)_3^{2+}$ (125 K)			$Ru(\eta^5\text{-}C_5H_5)(CH_3CN)_3^+$ (296 K)		
	uncorr	corr[b]		uncorr	corr[b]
Ru–N1	2.059 (2)	2.063 (2)	Ru–N1	2.085 (3)	2.091 (3)
Ru–N2	2.048 (2)	2.052 (2)	Ru–N2	2.082 (3)	2.089 (3)
Ru–N3	2.059 (2)	2.062 (2)	Ru–N3	2.083 (3)	2.090 (3)
$\langle$Ru–N$\rangle_{av}$	2.055 (4)	2.059 (4)	$\langle$Ru–N$\rangle_{av}$	2.083 (1)	2.090 (1)
N1–Ru–N2	86.33 (7)		N1–Ru–N2	85.9 (1)	
N1–Ru–N3	87.05 (7)		N1–Ru–N3	88.2 (1)	
N2–Ru–N3	84.67 (7)		N2–Ru–N3	87.7 (1)	
N1–C7	1.131 (3)	1.133 (3)	N1–C6	1.136 (4)	1.140 (4)
N2–C9	1.126 (3)	1.128 (3)	N2–C8	1.127 (4)	1.131 (4)
N3–C11	1.137 (3)	1.138 (3)	N2–C10	1.131 (4)	1.135 (4)
$\langle$N–C$\rangle_{av}$	1.131 (3)	1.133 (3)	$\langle$N–C$\rangle_{av}$	1.131 (3)	1.135 (3)
Ru–N1–C7	174.6 (2)		Ru–N1–C6	173.2 (3)	
Ru–N2–C9	175.9 (2)		Ru–N2–C8	174.7 (3)	
Ru–N3–C11	176.3 (2)		Ru–N3–C10	173.0 (3)	
C7–C8	1.453 (3)	1.456 (3)	C6–C7	1.438 (5)	1.443 (5)
C9–C10	1.450 (4)	1.453 (3)	C8–C9	1.452 (5)	1.457 (5)
C11–C12	1.449 (3)	1.451 (3)	C10–C11	1.444 (5)	1.449 (5)
$\langle$C–C$\rangle_{av}$	1.451 (1)	1.453 (1)	$\langle$C–C$\rangle_{av}$	1.445 (4)	1.450 (4)
Ru–C1	2.191 (2)	2.195 (2)	Ru–C1	2.134 (4)	2.140 (4)
Ru–C2	2.182 (2)	2.186 (2)	Ru–C2	2.139 (4)	2.145 (4)
Ru–C3	2.186 (2)	2.191 (2)	Ru–C3	2.141 (4)	2.147 (4)
Ru–C4	2.180 (2)	2.183 (2)	Ru–C4	2.132 (4)	2.139 (4)
Ru–C5	2.189 (2)	2.192 (2)	Ru–C5	2.127 (4)	2.134 (4)
Ru–C6	2.178 (2)	2.182 (2)	$\langle$Ru–C$\rangle_{av}$	2.135 (3)	2.141 (2)
$\langle$Ru–C$\rangle_{av}$	2.184 (2)	2.188 (2)	C_{plane}–Ru	1.777	1.781
C_{plane}–Ru	1.672	1.675			
C1–C2	1.397 (4)	1.399 (4)	C1–C2	1.401 (7)	1.406 (7)
C2–C3	1.415 (4)	1.418 (4)	C2–C3	1.404 (8)	1.408 (8)
C3–C4	1.393 (4)	1.395 (4)	C3–C4	1.373 (8)	1.378 (8)
C4–C5	1.418 (4)	1.420 (4)	C4–C5	1.403 (9)	1.407 (9)
C5–C6	1.399 (4)	1.401 (4)	C5–C1	1.376 (8)	1.381 (9)
C6–C1	1.415 (4)	1.417 (4)	$\langle$C–C$\rangle_{av}$	1.391 (7)	1.396 (7)
$\langle$C–C$\rangle_{av}$	1.406 (4)	1.408 (4)			
C6–C1–C2	119.1 (2)		C5–C1–C2	108.4 (5)	
C1–C2–C3	121.0 (3)		C1–C2–C3	107.2 (5)	
C2–C3–C4	119.1 (2)		C2–C3–C4	108.2 (5)	
C3–C4–C5	121.0 (2)		C3–C4–C5	108.4 (5)	
C4–C5–C6	119.1 (2)		C4–C5–C1	107.8 (5)	
C5–C6–C1	120.8 (2)				

[a] Numbering scheme shown in Figures 2 and 3. [b] Corrected for thermal motion; whole complex treated as rigid body.[12]

(22) Seiler, P.; Dunitz, J. D. *Acta Crystallogr.* **1980**, *B36*, 2946.
(23) Luginbühl, W.; Ludi, A.; Raselli, A.; Bürgi, H. B. *Acta Crystallogr.* **1989**, *C45*, 1428.

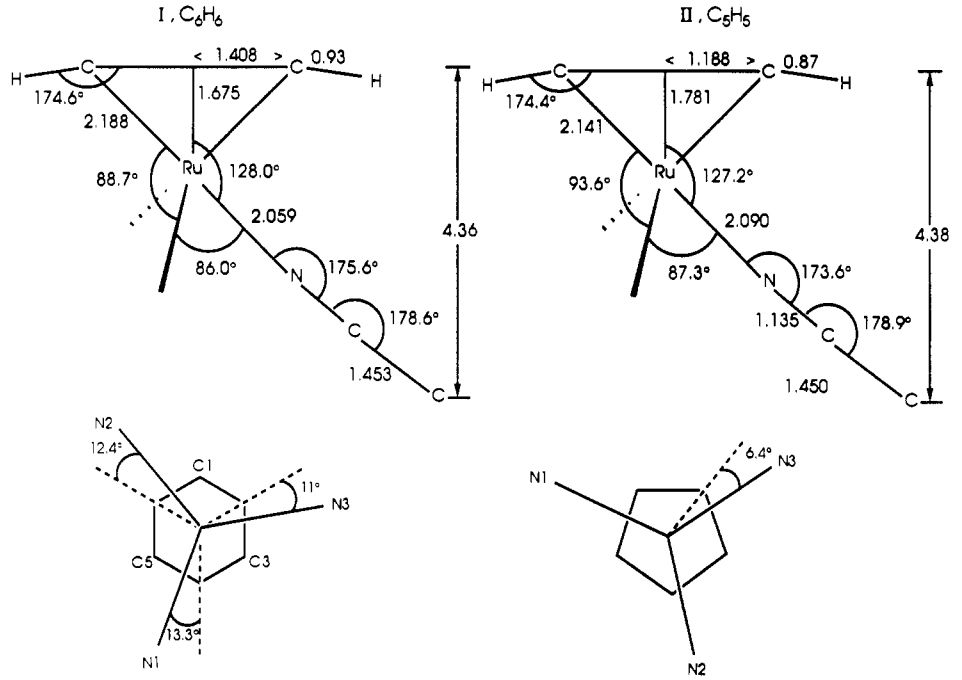

Figure 4. Comparison of the average geometries of $Ru(\eta^6\text{-}C_6H_6)(CH_3CN)_3^{2+}$ and $Ru(\eta^5\text{-}C_5H_5)(CH_3CN)_3^{+}$.

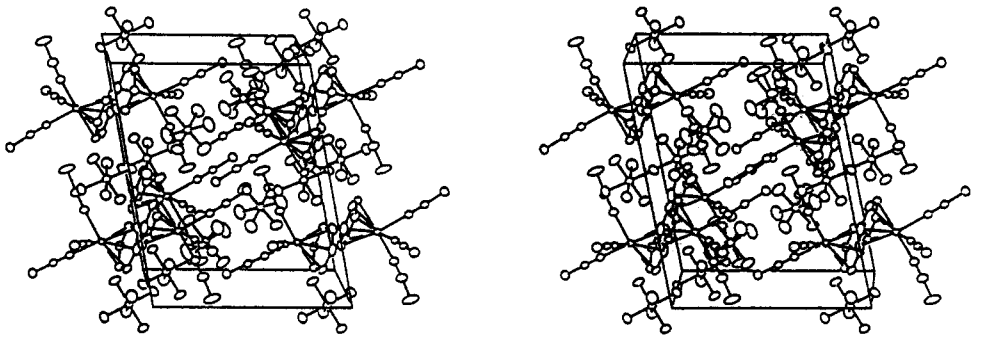

Figure 5. Stereoview of the unit cell of $[Ru(\eta^6\text{-}C_6H_6)(CH_3CN)_3](PF_6)_2$.

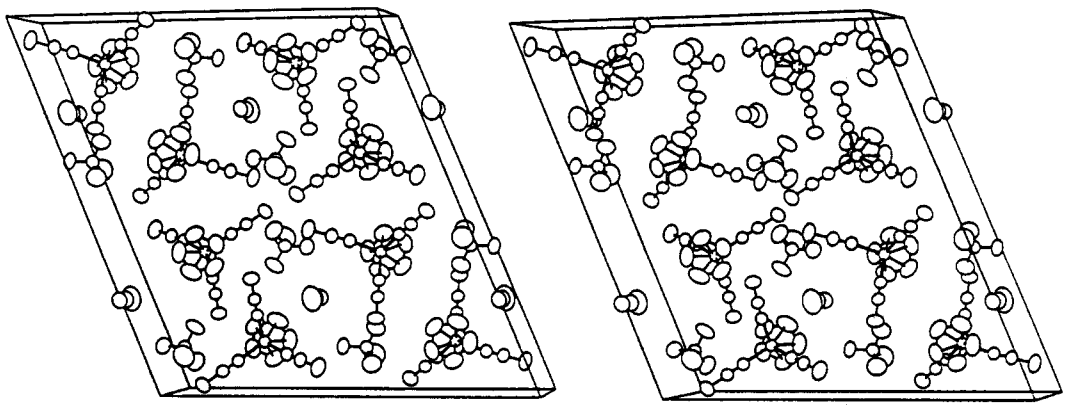

Figure 6. Stereoview of the unit cell of $[Ru(\eta^5\text{-}C_5H_5)(CH_3CN)_3]BF_4 \cdot 0.5CH_3CN$.

Table VI. Structure and Reactivity for Ru(II) Complex Ions with CH_3CN, $\eta^6\text{-}C_6H_6$, $\eta^5\text{-}C_5H_5^-$, and H_2O[a]

	$Ru(CH_3CN)_6^{2+}$	$Ru(\eta^6\text{-}C_6H_6)(CH_3CN)_3^{2+}$	$Ru(\eta^5\text{-}C_5H_5)(CH_3CN)_3^{+}$	$Ru(H_2O)_6^{2+}$	$Ru(\eta^6\text{-}C_6H_6)(H_2O)_3^{2+}$
Ru–L, Å	2.03	2.06	2.09	2.12	2.12
Ru–C_n center, Å		1.67	1.78		1.63
$k(CH_3CN \text{ or } H_2O)^{298}$, s^{-1}	8.9×10^{-11}	$4.07\ (2) \times 10^{-5}$	5.6 (2)	1.8×10^{-2}	11.5
ΔH^*, kJ mol^{-1}	140.3	102.5 (50)	86.5 (20)	87.8	75.9
ΔS^*, J K^{-1} mol^{-1}	33.3	15.0 (140)	59.6 (70)	16.1	29.9
ΔV^*, cm^3 mol^{-1}	0.4	2.4 (8)	11.1 (5)	−0.4	1.5
mechanism	I	I_d	D	I	I_d
ref	6, 23	this work	this work	6	4b

[a] Esd's in units of last significant digit.

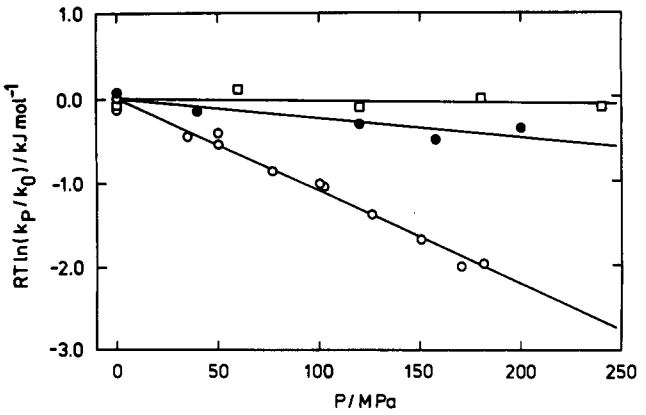

Figure 7. Pressure dependence of the CH_3CN-exchange rates k_p for $Ru(CH_3CN)_6^{2+}$ (□),[6] $Ru(\eta^6\text{-}C_6H_6)(CH_3CN)_3^{2+}$ (●), and $Ru(\eta^5\text{-}C_5H_5)(CH_3CN)_3^{+}$ (○). All solutions were 0.1 m in solute.

$(CH_3CN)_3^+$ by 5 orders of magnitude for each step. The increase correlates with a corresponding stepwise lengthening of the Ru–N distance by 0.03 Å. The kinetic (trans) effect thus correlates with the mutual (trans) influence of the ligands discussed in the preceding section. A qualitatively similar but quantitatively different structure–reactivity correlation is found for the analogous compounds where water takes the place of acetonitrile. Only two members of this series, however, have been studied, $Ru(\eta^5\text{-}C_5H_5)(H_2O)_3^+$ having not (yet) been prepared. Although the Ru–O distances for $Ru(H_2O)_6^{2+}$ and $Ru(\eta^6\text{-}C_6H_6)(H_2O)_3^{2+}$ are virtually identical, the water-exchange rates differ by 3 orders of magnitude; again the benzene complex shows the higher substitution lability and quite a short Ru–C distance (2.164 Å in $Ru(\eta^6\text{-}C_6H_6)(H_2O)_3^{2+}$, 2.225 Å in $Ru(\eta^6\text{-}C_6H_6)_2^{2+}$).[4b,6,21] These observations are attributed to a strong trans-labilizing influence of the π-acid benzene on the remaining three ligands. The influence is stronger for H_2O, which, unlike CH_3CN, does not participate in π-back-bonding.

A similar phenomenon is observed along the series $Cr(\eta^6\text{-}C_6H_6)_2$, $Cr(\eta^6\text{-}C_6H_6)(CO)_3$, and $Cr(CO)_6$, formally isoelectronic to our ruthenium compounds. The sign of the bond length change is just reversed, however. The (uncorrected) distance Cr–C for $Cr(CO)_6$ is 1.915 Å; for $Cr(\eta^6\text{-}C_6H_6)(CO)_3$ it is 0.073 Å shorter. The $Cr\text{–}C(C_6H_6)$ distance is 2.229 Å, 0.087 Å longer than that for $Cr(C_6H_6)_2$.[24] Consistent with this structural change, $Cr(\eta^6\text{-}C_6H_6)(CO)_3$ exchanges the aromatic ligand but not CO.[25] Analogous relationships between structure and activation parameters have been discussed in detail for several other reactions.[26]

In summary, we have demonstrated a variation of the substitution kinetics for the monodentate ligand by 12 orders of magnitude within a family of compounds of low-spin d^6 ruthenium(II) with a combination of the ligands H_2O, CH_3CN, C_6H_6, and $C_5H_5^-$ (Table VI). An empirical structure–reactivity relationship among the σ-donating/π-accepting capabilities of the ligands, the Ru–ligand distances, and the ligand substitution rates has been established.

From this data set we may speculate that the not yet existing compounds $Ru(\eta^5\text{-}C_5H_5)(H_2O)_3^+$ and *fac*-$Ru(CH_3CN)_3(H_2O)_3^{2+}$ should exchange water ligands very rapidly. Evidence for the occurrence of the latter species has been found in a recent solution study of the $Ru(H_2O)_6^{2+}$–acetonitrile system.[27]

Acknowledgment. We thank Ciba-Geigy for performing the microanalyses and Johnson Matthey for a loan of ruthenium chloride. This work was generously supported by the Swiss National Science Foundation (Grant Nos. 2.5'370.87 and 20-27.848.89).

Supplementary Material Available: Tables SI and SII (thermal parameters), SIII (interatomic distances and angles for PF_6^- and BF_4^-), and SIV and SV (hydrogen positions and isotropic displacement parameters (6 pages); tables of calculated and observed structure factors (8 pages). Ordering information is given on any current masthead page.

(24) Rees, B.; Coppens, P. *Acta Crystallogr.* **1973**, *B29*, 2515. Rees, B.; Mitschler, A. *J. Am. Chem. Soc.* **1976**, *98*, 7918. Keulen, E.; Jellinek, F. *J. Organomet. Chem.* **1966**, *5*, 490.
(25) Strohmeier, W.; Müller, R. *Z. Phys. Chem. Neue Folge* **1964**, *40*, 85.
(26) Bürgi, H. B.; Dubler-Steudle, K. *J. Am. Chem. Soc.* **1988**, *110*, 7291. *J. Am. Chem. Soc.* **1988**, *110*, 4953. Schwarzenbach, G.; Bürgi, H. B.; Jensen, W. P.; Lawrance, G. A.; Monsted, L.; Sargeson, A. M. *Inorg. Chem.* **1983**, *22*, 4029.
(27) Benvenuti, M.; Merbach, A. E. Unpublished results.